



MFB-LANN: A lightweight and updatable myocardial infarction diagnosis system based on convolutional neural networks and active learning



Ziyang He, Zhiyong Yuan*, Panfeng An, Jianhui Zhao, Bo Du

School of Computer Science, Wuhan University, Wuhan 430072, China

ARTICLE INFO

Article history:

Received 16 January 2021

Accepted 24 August 2021

Keywords:

Myocardial infarction (MI)
Convolutional neural networks (CNN)
Lead attention mechanism (LAM)
Active learning (AL)
Real-time diagnosis

ABSTRACT

Background and objectives: 12 leads electrocardiogram (ECG) are widely used to diagnose myocardial infarction (MI). Generally, the symptoms of MI can be reflected by waveforms in the heartbeat, and the contribution of different ECG leads to different types of MI is different. Therefore, it is significant to use the heartbeat waveform features and the lead relationship features for multi-category MI diagnosis. Moreover, the challenge of individual differences and lightweight algorithms also need to be further resolved and explored in the ECG automatic diagnosis system.

Methods: This paper presents a lightweight MI diagnosis system named multi-feature-branch lead attention neural network (MFB-LANN) via 12 leads ECG signals. It is designed based on the characteristics of the ECG lead. Specifically, 12 independent feature branches correspond to different leads, and each branch contains different convolutional layers to extract features in the heartbeat, then a novel attention module is developed named lead attention mechanism (LAM) to assign different weights to each feature branch. Finally all the weighted feature branches are fused for classification. Furthermore, to overcome individual differences, patient-specific scheme and active learning (AL) are used to train and update the model iteratively.

Results: Experimental results based on Physikalisch-Technische Bundesanstalt (PTB) database shows that the MFB-LANN achieved satisfactory results with accuracy of 99.63% based on 5-fold cross validation under the intra-patient scheme. The patient-specific experiment yielded an average accuracy of 96.99% compared to the state-of-the-art. By contrast, the model achieved acceptable results on the hybrid database (PTB and PTB-XL), especially achieving 94.19% accuracy after the update. Moreover, the system can complete the update process and real-time diagnosis on the ARM Cortex-A72 platform.

Conclusions: Experiments show that the proposed method for MI diagnosis has more obvious advantages compared to other recent methods, and it has great potential to be applied to the mobile medical field.

© 2021 Elsevier B.V. All rights reserved.

1. Introduction

Myocardial infarction (MI) is one of the heart diseases with high mortality. It occurs due to coronary occlusion and interruption of blood flow, resulting in partial myocardial necrosis because of severe persistent ischemia [1]. Cardiac activity produces electricity that passes through the tissues and body fluids from the heart to the surface of the body at different parts of the body. Electrocardiogram (ECG) is drawn by the current and usually collected along 12 leads, including I, II, III, aVR, aVL, aVF, and V1-V6. Each lead views the heart at a unique angle, which can reflect the condition

of different parts of the heart [2]. A heartbeat signal typically includes different features such as QT interval, ST-segment, P, QRS, and T waves, and it could directly reflect the electrical activity of the heart. However, ECG is a weak physiological signal, resulting in the feature extraction process is time-consuming. Moreover, MI is a complex heart disease, and it can be divided into many types based on the location of the disease, such as anterior MI (AMI), anteroseptal MI (ASMI), anterolateral MI (ALMI), inferior MI (IMI), and inferolateral MI (ILMI). Experienced doctors need to combine 12 leads ECG signals to diagnosing multi-class MI accurately [3]. However, the manual diagnosis process is time-consuming, resulting in many clinical ECG not being processed promptly. Therefore, it is crucial to propose a reliable method that can diagnose MI automatically and efficiently.

* Corresponding author.

E-mail address: zhiyongyuan@whu.edu.cn (Z. Yuan).

Research on ECG signal diagnostic methods has been developed for decades. Many researchers use methods based on traditional machine learning (ML) to diagnose MI. The process usually involves data preprocessing, extracting features, and building classifiers. ECG signals usually contain many types of noise, such as power line interference, baseline wander, and electrode contact noise [4]. These noises significantly impact the feature extraction, so they must be removed by different filters, such as band-pass filters, low-pass filters, high-pass filters, and median filters. In the feature extraction stage, some researchers manually extract waveform features with noticeable MI performance in ECG based on medical experiences, such as QRS-waves, ST-segment, and ST-T complex. Also, some researchers use mathematical transformation to extract new MI ECG features. For example, Zhang et al.[5] constructed an effective ECG tensor containing multi-dimensional association information from 12-lead ECG signals based on discrete wavelet transform. Then, the multi-lead feature extraction algorithm based on parallel factor analysis is developed to automatically extract the low-dimensional and highly recognizable lead characteristic features of the tensor. Finally, the extracted features are input to a bagged decision tree for MI localization. The mostly used classifiers are support vector machine (SVM) [2,6–11], k-Nearest Neighbor (KNN) [6,7,12], decision trees [6]. However, manually extracting features is an obvious drawback because it seriously affects the accuracy of the classifier, and useful ECG features are challenging to obtain and highly depend on clinical diagnostic experience. Besides, missing important information in the process of the handcrafted feature extraction may lead to misdiagnosis [13].

On the other hand, the entire ECG classification process based on deep learning (DL) is automatic without manually analyzing and extracting features. DL techniques have achieved remarkable success in medical fields, such as medical image recognition, case information analysis, and physiological signal detection. Most researchers have focused on using neural networks for MI diagnosis. For example, Acharya et al. [14] designed an 11-layer deep network using single-lead ECG singles for MI detection, and the model achieved an accuracy of 95.22%. Furthermore, Han et al. [15] proposed a multi-branch model based on residual network to diagnose MI using 12 leads ECG data, and the accuracy of the model for MI detection and MI localization reached 99.92% and 99.72% respectively. Baloglu et al. [16] designed a deep learning model with an end-to-end structure, which yielded impressive accuracy and sensitivity performance over 99.00% for MI multi-category diagnosis on 12 leads ECG signals. Based on the above work, most neural network models have achieved good results for MI diagnosis. However, methods based on deep learning usually have higher requirements for the training environment and computing platform, limiting the application scenarios of the automatic diagnosis system. Therefore, it is worth exploring the lightweight neural network model and building an MI diagnosis system on resource-constrained devices.

Besides, individual differences between patients are challenging in ECG diagnosis. Its related research needs to be further explored, especially for MI multi-class diagnosis. For example, some methods only achieved good results in intra-patient experiments because the data in the training set and test set may come from the same patients, which does not mean that the models can achieve the same effect on new patient data. Also, although some authors have conducted experiments under the inter-patient scheme, the results show that most algorithms cannot effectively overcome individual differences [15,17,18]. For example, the model in [15] only achieved an accuracy of 55.74% for MI multi-class diagnosis. Therefore, the training pattern based on patient-specific scheme is used by many researchers, which allows adding expert experience to fine-tune the model. For example, Liu et al.[19] used the first 32 heartbeats

to be selected from the records of each new patient in the test set to fine-tune the model, the diagnostic effect on new patients is greatly improved. However, sequential sampling cannot guarantee that the selected data are the most contributory for model optimization, and it may lead to manual labeling of some useless samples.

To address the challenges mentioned above, we propose a lightweight MI diagnosis system based on DL named multiple-feature-branch lead attention neural network (MFB-LANN), which can automatically diagnose multi-category MI using 12 leads ECG signals. The proposed model can obtain the features in the heartbeat of each lead and the weight contribution of different leads. Compared with other methods, it can overcome the individual differences of ECG through iterative update and achieve state-of-the-art performance. Moreover, the model update process and real-time diagnosis process can be completed on resource-constrained edge devices. The contributions of this work are listed as follows:

- To fully extract the features of 12 leads, a multiple-feature-branch (MFB) module is designed. It contains 12 independent feature branches consisting of convolution and pooling functions. Also, a novel method named lead attention mechanism (LAM) is proposed, which can learn the importance of different leads for different categories. The features of all leads are summarized for the final diagnosis.
- To overcome the individual differences, training strategies based patient-specific scheme and active learning (AL) are performed. For ECG signals of new patients, the most representative samples are selected based on uncertainty sampling strategy to update and optimize the model iteratively. It can reduce the cost of manual labeling and further improve the effectiveness of the model.
- Compared with published literatures, the proposed system has fewer parameters and computational complexity while maintaining very competitive accuracy. It can be deployed on resource-constrained edge devices to complete the model update and real-time MI diagnosis.

The paper is organized as follows: Section 2 introduces the dataset and pre-processing. The principle of the proposed method is illustrated in Section 3. Section 4 shows the experiments and results. In Section 5, detailed discussions are presented. Finally, the conclusion is given in Section 6.

2. Dataset and pre-processing

In this paper, all the ECG data used comes from Physikalisch-Technische Bundesanstalt (PTB) diagnostic ECG database [20] and PTB-XL [21] ECG database.

The PTB database contains a total of 549 ECG records from 290 patients. Each patient is represented by one to six records, and each record is at least 30s. Cardiologists have labeled all records, and every record includes 12 conventional leads (I, II, III, aVR, aVL, aVF, and V1-V6) and 3 frank leads (VX, VY, and VZ). The sampling rate of the signal is 1000Hz. In this paper, we selected ECG records from 113 MI patients (including AMI, ASMI, ALMI, IMI, and ILMI) and 52 Healthy controls (HC) patients to evaluate the MFB-LANN.

The PTB-XL ECG dataset is a large dataset of 21,837 clinical 12 conventional leads ECG records from 18,885 patients. The length of each record is 10s and the data have been labeled by cardiologists. The database contains 71 types of heart diseases and most records may contain multiple annotations. The sampling rate of the data is 500Hz. Consistent with PTB, we extracted 2184 normal records and 3201 records containing 5 types of MI.

All records are downsampled to 250Hz to reduce the calculation cost. Then, denoising based on wavelet transform is performed. Also, the Pan-Tompkins [22] algorithm is used to locate the R peak

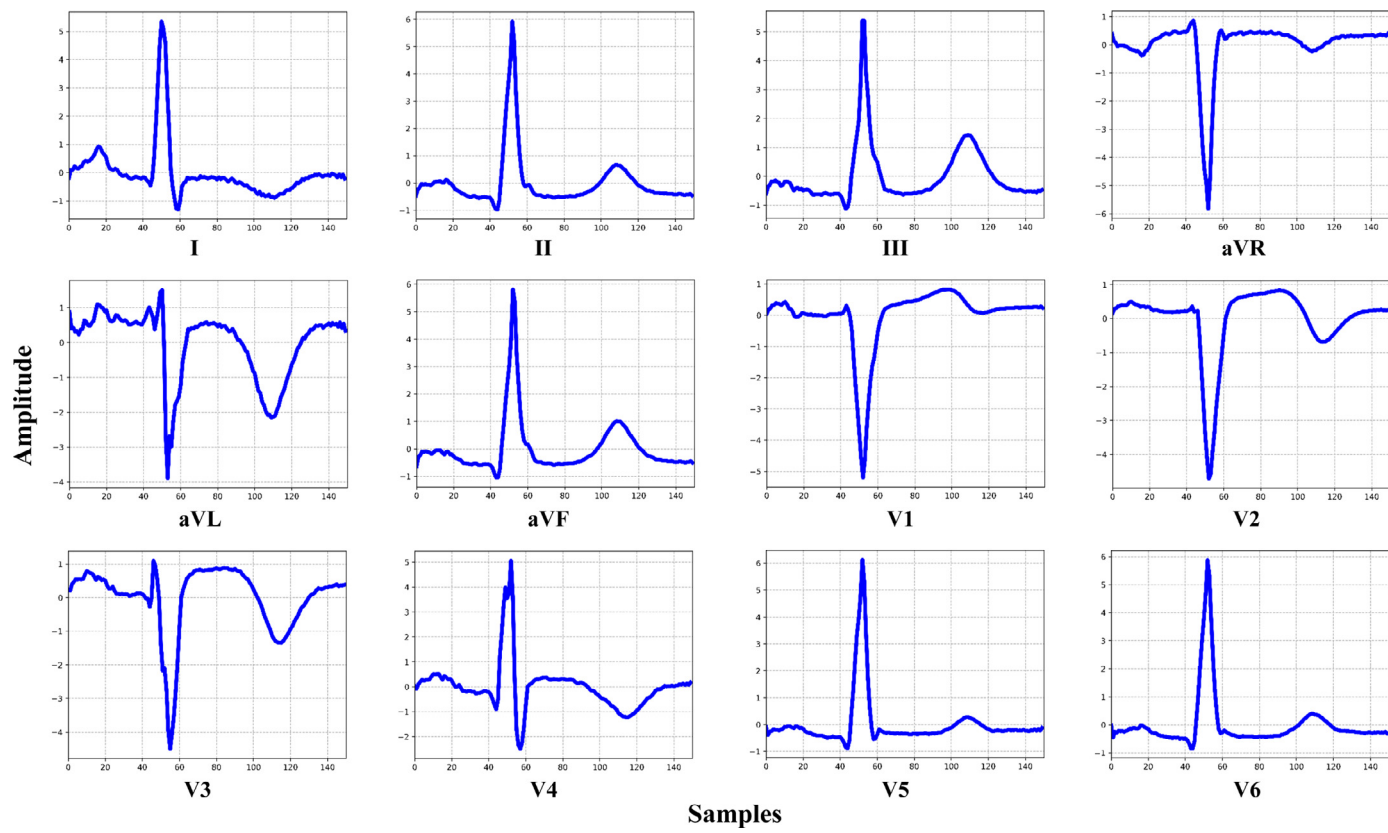


Fig. 1. 12 leads ECG heartbeats after pre-processing.

Table 1

Summary of PTB dataset used in the paper.

Class	No. of subjects	No. of records	No. of 12 leads heartbeats
AMI	17	44	6517
ASMI	27	72	11,515
ALMI	16	40	6668
IMI	30	83	12,749
ILMI	23	51	8172
HC	52	70	10,614
Total	165	360	56,235

and select 0.2 seconds (50 samples) before the R peak and 0.4 (99 samples) seconds after the R peak as a heartbeat sample, which can effectively help the model locate the disease features and improve diagnostic accuracy. Furthermore, Z-score is used to normalize each heartbeat because it can eliminate the offset effect and standardize the ECG signal amplitude to benefit the model training [14]. The calculation is as follows:

$$Z = \frac{X - \mu}{\delta} \quad (1)$$

where X denotes the beat, μ and δ are the mean value and standard deviation of the beat, respectively. A typical MI heartbeat is shown via pre-processing in Fig. 1. Table 1 and Table 2 show the details of the data after preprocessing.

3. Method

As mentioned before, ECG signals in different leads can reflect the conditions of different parts of the heart. Clinical practice has proved that the 12 leads combination can diagnose MI more comprehensively than using single-lead [3]. Further, according to the

Table 2

Summary of PTB-XL dataset used in the paper.

Class	No. of subjects	No. of records	No. of 12 leads heartbeats
AMI	113	116	1405
ASMI	1310	1528	18,507
ALMI	171	201	2409
IMI	909	1025	12,267
ILMI	281	331	3923
HC	1967	2184	21,854
Total	4751	5385	60,365

MI diagnostic rules and leads interpretation [2,3], the characteristics of ECG leads can be summarized as follows:

Specificity: 12 leads are located in different parts of the body, and they are independent of each other.

Similarity: In a heartbeat cycle, all ECG signals originate from the same heart activity, so the waveform change law in all leads is similar.

Integrity: Some specific diseases can only be reflected by certain leads, which requires all lead information for final diagnosis.

The architecture of MFB-LANN is designed based on the above characteristics. As shown in Fig. 2, first, due to the specificity and similarity of the leads, the preprocessed 12 leads ECG data is input into the corresponding 12 separate convolution branches. Still, they have the same convolution structure, convolution kernel size and number of convolution kernels. Then, LAM assigns different weights to each feature branch to strengthen the essential features and weaken the other branches. Finally, the features of all branches are fused for classification based on the integrity of the ECG. Fig. 3 shows the detailed network structure of the proposed model for MI localization, including the detailed internal structure of each module, the sizes of the input and output of each layer. Moreover,

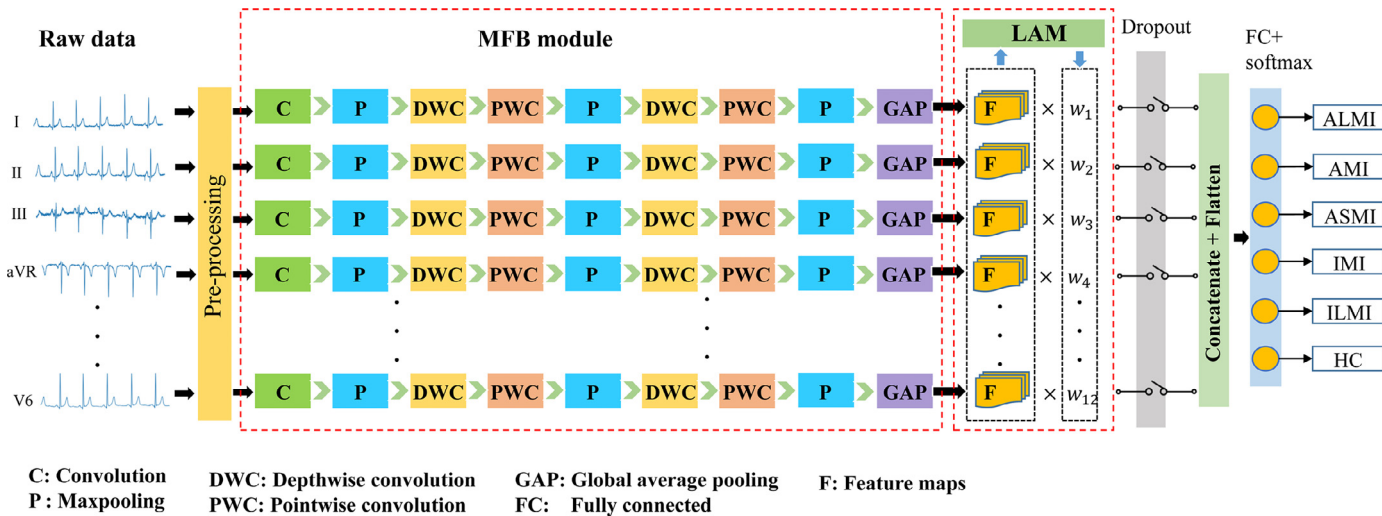


Fig. 2. The architecture of the proposed MFB-LANN.

Table 3
Detailed structural information of each feature branch.

Layer	Kernel/Pool size	No. of kernel
C	17	4
P-1	3	-
DWC-1	9	4
PWC-1	1	8
P-2	2	-
DWC-2	5	8
PWC-2	1	16
P-3	2	-
GAP	12	-

C: Traditional convolutional; P: Pooling; DW: Depthwise convolution; PW: Pointwise convolution; GAP:Global average pooling.

patient-specific scheme and AL are used to build and update models to overcome individual differences. The details of each part are illustrated as follows.

3.1. MFB Module

As shown in Fig. 2, the MFB module mainly performs feature extraction and dimensionality reduction through traditional convolutional layer, depthwise separable convolutions layer, pooling layer, and (global average pooling) GAP layer. Convolutional neural network (CNN) has achieved excellent results in the field of computer vision because its 2-dimension (2-D) convolution kernel can extract abstract and effective features on pictures. However, although the multi-lead ECG data can also be changed to a multi-dimensional structure when represented by a numeric matrix, 2-D convolution kernels are not suitable to be used to filter it because the data relationship between and within leads is different from the relationship between adjacent pixels in the image. Therefore, the convolution kernels used are modified to the 1-dimension (1-D) in this paper. Moreover, depthwise separable convolution is adopted because it can effectively reduce the model parameters and calculations by depthwise convolution (DWC) and pointwise convolution (PWC) [23]. Going further, maxpooling operations are used to reduce feature dimensions without learning any parameters. Finally, GAP can regularize the structure of the entire feature branch to prevent overfitting.

Table 3 summarizes the internal structure of a single feature branch module. As the network depth increases, the convolution

kernel keeps getting smaller to adapt to the size change of the feature map during dimensionality reduction. The number of convolution kernels is increased to obtain more abstract features.

3.2. LAM Module

Attention mechanism has become an important optimization structure of the neural network, and it has achieved excellent performance in the fields of neural machine translation [24] and computer vision [25]. The principle is similar to the attention function of the human brain. It can help the model pay more attention to the learning of the target area in image recognition. Also, attention structure promotes the interpretability of neural networks. In this paper, based on ECG lead characteristics and MI diagnosis rules, we propose a new attention architecture named LAM to optimize the model. Its principle is shown in Fig. 4. First, the number of features from each feature branch is compressed to 1 by a 1x1 size convolution kernel and ReLU function, which can reduce the input dimension of the next layer (FC) to reduce the parameters and computational complexity. Then a fully connected layer (the number of neurons is 12) and a sigmoid function are designed to generate a weight vector. The output features of each lead are multiplied by corresponding weights. The implementation process of LAM can be summarized by Eq. (2)-(4).

$$V_i = f_{re}(f_{co}(X_i)) \quad (2)$$

$$W_i = f_{sg}(f_{fc}([V_1, V_2, \dots, V_{12}])) \quad (3)$$

$$O = f_{cy}(W_i) \odot X_i \quad (4)$$

here, X_i denotes the feature vector of each lead, i represents the i th lead, f_{co} and f_{re} denote the convolution operation and rectified linear unit (ReLU) [26] function, respectively. $[V_1, V_2, \dots, V_{12}]$ means the combination of feature vectors of 12 leads, f_{sg} and f_{fc} are sigmoid activation function and fully connected (FC) operation, W_i denotes weight vector, f_{cy} is a copy operation to share each weight to the same dimension as X_i , \odot means an element-wise multiplication between matrices. O represents the weighted feature vector of each branch. LAM can automatically obtain the importance of each feature branch, and then strengthen useful feature branches and weaken other branches.

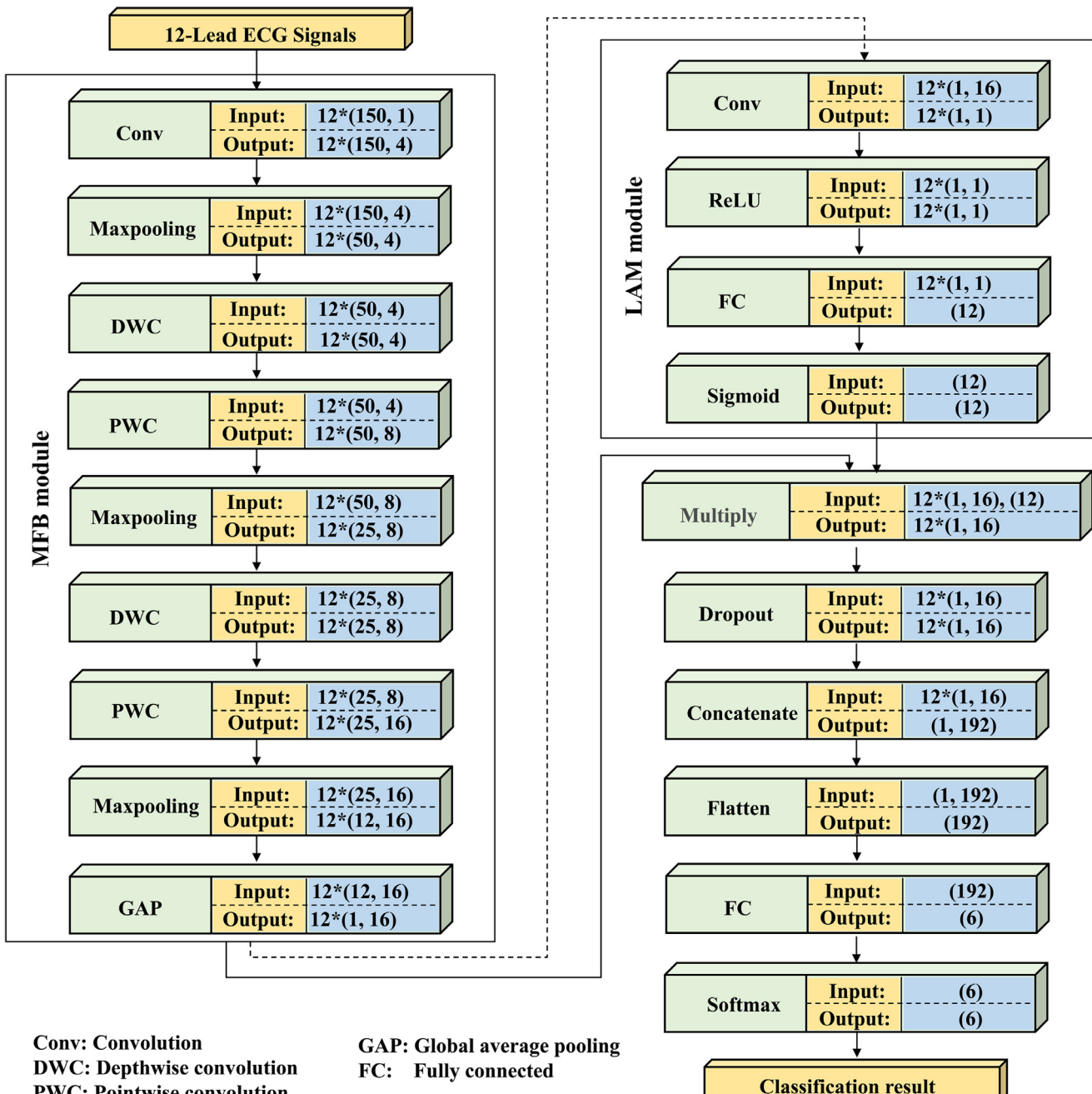


Fig. 3. The detailed network structure of the proposed model.

3.3. Information fusion

Dropout [27] is a commonly used regularization method in neural network. It can randomly drop some neurons to prevent overfitting. As shown in Fig. 2, we add a dropout layer before combining the 12 feature branches and set the value to 0.5. It means that the network has a variety of combined structures to enhance the generalization ability. Then, the concatenation and flattening operation is used for the output of 12 branch features, and the formula is expressed as:

$$\text{Output} = f_{\text{fla}}(f_{\text{con}}(M_1, M_2, M_3 \dots, M_{12})) \quad (5)$$

M_i represents the output vector of each feature branch, its dimension is 1x16, and i represents the i -th feature branch. f_{con} represents the concatenation operation. It combines the vectors of dif-

ferent feature branches, and the output dimension is 1x192. The f_{fla} operation changes the data shape to 192. Finally, all feature vectors are integrated by FC, and the probabilities of six categories are output through the softmax function.

3.4. Training and update strategy

In real-world applications, computer-aided diagnostic algorithms inevitably need to diagnose ECG of new patients, and individual differences are one of the main challenges [15]. Thus, methods based on patient-specific scheme have been developed to overcome the problem [28,29]. It allows the algorithm to "peek" a part of the new patient data to learn the data feature of the specific patients. The detailed process is shown in Fig. 5(a). First, a training set composed of different patients is used to pre-training the

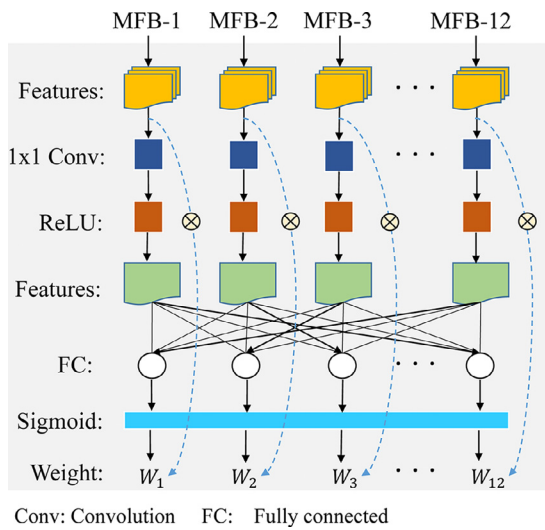


Fig. 4. The architecture of the LAM. The operation is illustrated as Eq. (2)-(4).

model globally to learn the overall features of the data. Then, for the new patient who need to be diagnosed, select some samples to fine-tune the model, which can adapt the model to the new patient ECG characteristics and overcome individual differences. In this article, AL [30,31] is integrated into the patient-specific scheme to update the model.

AL is a machine learning setup that enables machines to cleverly ask questions to reduce the labeling efforts [32]. For a large number of unlabeled samples pool, the purpose of AL is to select the sample with the highest contribution and manually label them to the optimization model. It can make the model reach the desired effect faster with fewer data and reduce manual annotation costs. In this paper, AL is used to update the proposed model continuously, and the specific process is shown in Fig. 5(b). The new patient ECG data serves as the initial unlabeled data pool. In each iteration, the most useful samples of each patient in the data pool are selected according to the ranking strategy. The selected sample is labeled by the cardiologist and added to

the patient-specific training set in the current iteration. Then the labeled patient-specific training set is used to update the current model. The remaining samples in the unlabeled data pool are used as the new data pool and enter the next iteration. The update process ends when the stop condition is reached.

Uncertainty is a commonly used data selection criterion in AL [33]. In multi-classification tasks, it can be expressed as:

$$\text{Uncertainty} = 1 - \text{argmax}_P(i) \quad (6)$$

$P(i)$ is defined as the posterior probability obtained for each class by the MFB-LANN, where i is the number of classes. $\text{argmax}_P(i)$ represents the largest posterior probabilities among all classes. In six classification, if the posterior probabilities of two samples are (0.85, 0.03, 0.03, 0.03, 0.03) and (0.5, 0.1, 0.1, 0.1, 0.1), the uncertainty value are 0.15, 0.5 respectively. From the posterior probability distribution, it can be inferred that the model has a high uncertainty for the latter. Thus, samples with larger *Uncertainty* should be labeled to optimize the model.

In this article, for each new patient data, we select the first 10 samples with higher uncertainty in each iteration and add them to the patient-specific training set. Moreover, the iteration is stopped when the iteration process reaches ten times. The [Algorithm 1](#) gives the main steps of the model training and update process based on patient-specific scheme and AL.

4. Experiments and results

4.1. Experimental platform and basic settings

Experimental studies for MI diagnosis under intra-patient scheme and patient-specific scheme are implemented with the proposed model. The model structure and initial parameters are not changed, only the data set division method is changed. Also, Adam [34] is used as an optimizer. The epoch and batch-size are 60 and 128, respectively. The initial learning rate is set to 0.001, which is changed every 15 epochs. In contrast, the model update is a fine-tuning training process with a small number of samples, and its epoch, batch-size and initial learning rate are 40, 32, 0.002, respectively.

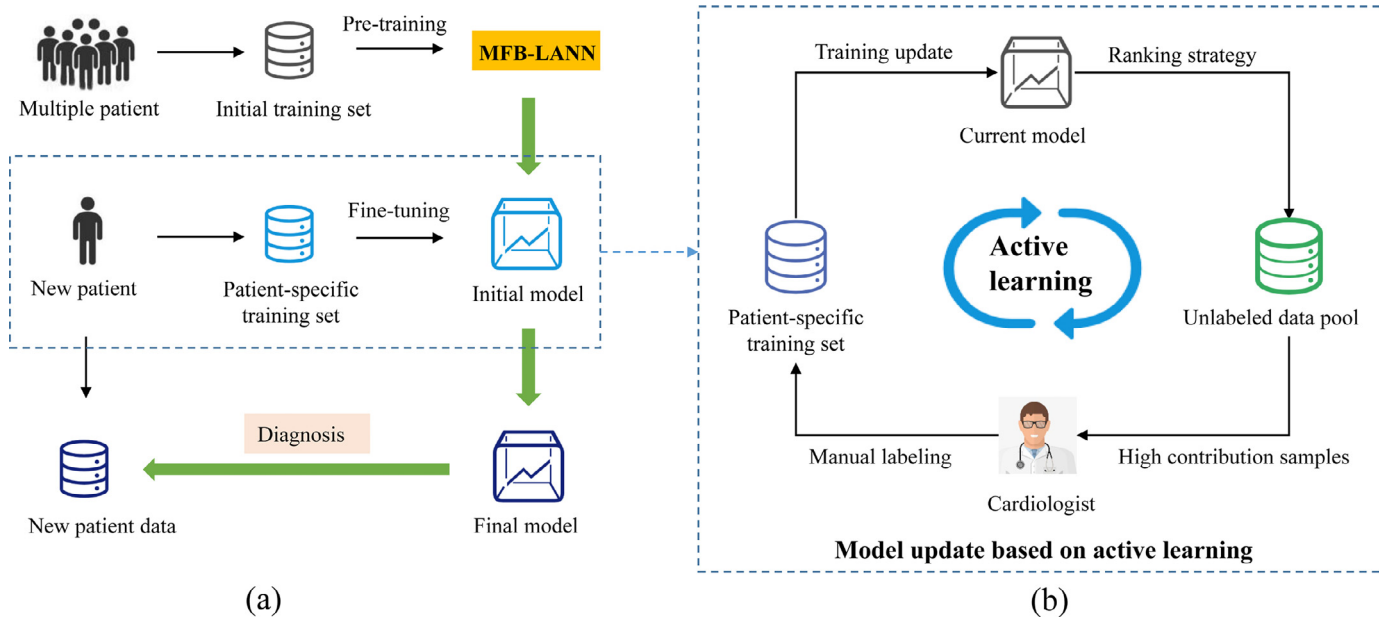


Fig. 5. Model training and update based on patient-specific scheme and AL. (Figure (a) is the training process based on the patient-specific scheme, Figure (b) shows that the model update is based on AL).

Algorithm 1 Model training and update based on patient-specific scheme and AL.

Input: ~

Initial training set, G ;
Unlabeled data pool, T ;
Patient-specific training set, D ;
Active learning iterations: L ;
Number of samples to label at each iteration: N ;

Output: ~

Final model;
1: Train an initial model M based on initial training set G ;
2: **for** $i = 0$; $i < L$; $i++$ **do**
3: Calculate the posterior probability of each sample in unlabeled data pool T using the model M ;
4: Calculate the *uncertainty* value of the unlabeled samples T using Eq. (6);
5: Rank the unlabeled samples based on *uncertainty* values;
6: Ask the cardiologist to label the top N samples;
7: Add labeled samples to the patient-specific training set D ;
8: Update model M using the patient-specific training data set D ;
9: Delete the labeled samples in unlabeled data pool T ;
10: **end for**
11: **return** Model M ;

The whole network is developed based on TensorFlow, a prevalent deep learning framework. The experiments were performed on an AI server with Intel Core i5-7640X@4.00GHz CPU and 32 GB RAM. Also, to prove the lightweight advantages of the model, the model is deployed on resource-constrained edge devices in [Section 5.2](#).

4.2. Performance evaluation

For a comprehensive performance evaluation, the proposed model is evaluated by Accuracy (Acc), Sensitivity (Se), Specificity (Sp), Positive predictivity (Pp), F-measure (F1). They are defined as follows:

$$Acc = \frac{TP + TN}{TP + TN + FP + FN} \quad (7)$$

$$Se = \frac{TP}{TP + FN} \quad (8)$$

$$Sp = \frac{TN}{TN + FP} \quad (9)$$

$$Pp = \frac{TP}{TP + FP} \quad (10)$$

$$F1 = \frac{2 * Se * Pp}{Se + Pp} \quad (11)$$

where TP and TN represent the number of true positive and true negative patients, respectively. FN and FP indicate the quantity of false negative and false positive.

4.3. Experimental results on PTB

In this subsection, we only use the PTB database to perform experiments based on intra-patient and patient-specific schemes.

Table 4

5-fold cross validation results based on intra-patient scheme using PTB.

Fold	Acc (%)	Se (%)	Sp (%)	Pp (%)	F1 (%)
1	99.61	99.60	99.92	99.54	99.57
2	99.66	99.63	99.93	99.61	99.62
3	99.62	99.61	99.92	99.54	99.58
4	99.76	99.74	99.95	99.70	99.72
5	99.52	99.48	99.91	98.42	99.45
Average	99.63	99.61	99.93	99.56	99.59

4.3.1. Intra-patient scheme

To obtain more credible results, 5-fold cross validation is used to evaluate the model. [Table 4](#) and [Table 5](#) summarize the experimental results. It is obvious that our model achieved excellent performance on MI multi-category diagnosis under intra-patient scheme. It can be seen from [Table 4](#) that the average Acc, Se, Sp, Pp, and F1 reached 99.63%, 99.61%, 99.93%, 99.56%, 99.59% respectively. For each fold, the Acc is above 99.5%. Especially in the fourth fold experiment, only 0.24% heartbeats are misclassified, reflecting the superiority of the model. The result of each iteration experiment has a small difference, and it proves the robustness of the model. [Fig. 6](#) shows the accuracy and loss changes of the training set and validation set during the model training process. The performance improved rapidly in the first 20 epochs and the model began to converge at about the 45th epoch. According to the changes of the training curve and the validation curve, the model achieves good fit without overfitting or underfitting. Moreover, the confusion matrix is shown in [Table 5](#), only 0.37% heartbeats are misclassified. From the confusion matrix distribution, it is relatively difficult for the model to distinguish between ALMI, AMI and ASMI or between ILMI and IMI. This is probably because diseases in similar locations can easily produce the same waveform symptoms, and it increases the difficulty of model differentiation, but the Acc of ALMI still reached 99.82%. Overall, impressive results are obtained, manifesting as high Acc, Se, Sp, Pp, and F1. It can prove that the proposed model has a strong fitting ability for MI diagnosis using 12 leads ECG.

4.3.2. Patient-specific scheme

As mentioned before, the individual differences between patients have a strong negative impact on models. Thus, experiments based on patient-specific scheme with AL are performed in this subsection. Different from intra-patient scheme, the PTB database is divided by patients. Also, to ensure that there are sufficient samples to update the model during the iteration, 40 patients data with relatively long-lasting records are divided into the unlabeled data pool and test set. For each patient, 400 samples are randomly selected and added to the unlabeled data pool, and the remaining samples are added to the test set. Finally, the numbers of the unlabeled data pool and the test set are 16,000 and 7947, respectively.

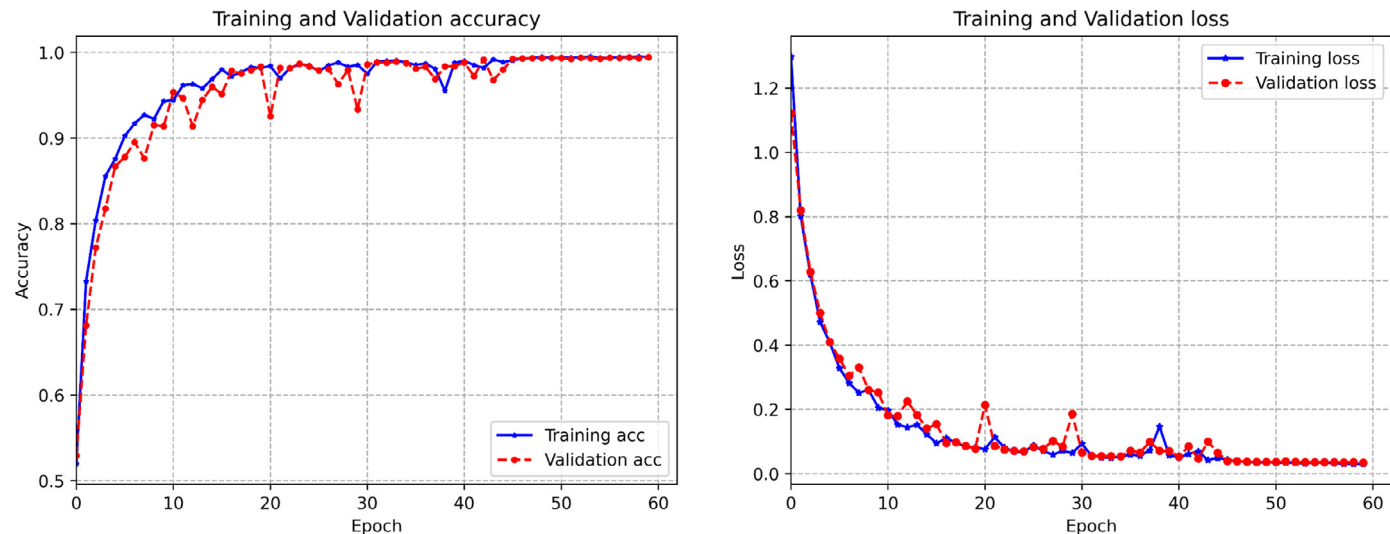
[Table 6](#) shows the detailed confusion matrix classification results. From the overall results, we can see that Acc, Se, Sp, Pp and F1 have reached 96.99%, 96.86%, 99.40%, 96.87% and 96.87%, respectively. Although individual differences negatively impact the model, the result is still acceptable after updating and optimization, and the Acc of each category exceeds 99%. Therefore, it can be concluded that the model has adapted to the characteristics of the new patient data and limited the negative impact of individual differences within the acceptable range based on the patient-specific scheme.

The model update process based on AL is shown in [Table 7](#). In each iteration, the 10 most uncertain samples for each new patient are selected and labeled to update the model. In this paper, the labels in the database are regarded as expert labels. When the

Table 5

Confusion matrix and performance across 5-fold cross validation based on intra-patient scheme using PTB.

	ILMI	Predicted						Performance				
		IMI	Acc (%)	Se (%)	Sp (%)	Pp (%)	F1 (%)	Acc (%)	Se (%)	Sp (%)	Pp (%)	F1 (%)
True	HC	10,603	6	1	2	3	4	99.95	99.85	99.98	99.90	99.87
	ALMI	3	6614	26	17	3	0	99.82	99.26	99.89	99.19	99.23
	AMI	1	18	6467	2	1	2	99.87	99.63	99.90	99.23	99.43
	ASMI	3	20	20	11,495	8	1	99.87	99.55	99.95	99.81	99.68
	ILMI	2	3	3	0	8125	16	99.88	99.71	99.95	99.44	99.57
	IMI	2	7	0	1	31	12,725	99.89	99.68	99.90	99.82	99.75
		Overall						99.63	99.61	99.93	99.56	99.59

**Fig. 6.** Training (blue lines) and validating (red lines) performance graphs based on intra-patient scheme using PTB. (For interpretation of the references to colour in this figure legend, the reader is referred to the web version of this article.)**Table 6**

Confusion matrix and performance based on patient-specific scheme using PTB.

		Predicted						Performance				
		HC	ALMI	AMI	ASMI	ILMI	IMI	Acc (%)	Se (%)	Sp (%)	Pp (%)	F1 (%)
True	HC	852	0	3	5	3	0	99.70	98.73	99.82	98.50	98.61
	ALMI	0	1043	45	21	0	5	98.46	93.63	99.25	95.34	94.47
	AMI	8	27	1062	13	0	5	98.53	95.25	99.06	94.32	94.78
	ASMI	2	16	11	1543	3	2	99.04	97.84	99.34	97.35	97.60
	ILMI	0	3	0	1	1365	25	99.23	97.92	99.51	99.51	97.81
	IMI	3	5	5	2	26	1843	99.02	97.82	99.39	99.39	97.93
		Overall						96.99	96.86	99.40	96.87	96.87

Table 7

Model update based on patient-specific scheme using PTB.

Labeled	Acc (%)	Se (%)	Sp (%)	Pp (%)	F1 (%)
0	54.88	57.22	91.06	53.07	52.23
10	62.64	61.63	92.33	65.45	62.18
20	81.18	80.51	96.15	81.97	80.50
30	90.65	90.32	98.10	90.91	90.55
40	93.18	92.72	98.62	93.29	92.87
50	94.78	94.29	98.96	94.33	94.30
60	95.39	95.07	99.08	94.94	95.00
70	95.94	95.67	99.19	95.58	95.62
80	96.50	96.29	99.30	96.22	96.25
90	96.88	96.68	99.38	96.64	96.66
100	96.99	96.86	99.40	96.87	96.87

number of patient-specific training sets is 0, it can be seen that the Acc, Se, Sp, Pp and F1 of the model are only 54.88%, 57.22%,

91.06%, 53.07%, and 52.23%. It can be inferred that individual differences have a great negative impact on the model. During the update, the recognition ability of the model continues to improve in the process of learning specific patient data. Also, in order to prove the advantages of selecting data based on uncertainty strategies, two other data selection methods are performed for comparison, namely sequential sampling and random sampling. The former refers to selecting the first 10 samples of the new patient to add the patient-specific training set during each iteration, the latter is randomly selected data. Fig. 7 shows the Acc and F1 of different methods during the model update process. It can be seen that the method based on uncertainty strategy is better than other methods in the optimization process. The relatively poor method is sequential sampling because it is difficult to ensure that the samples selected are the most contributory to the model. In general, AL can further improve the generalization ability of the model, and it re-

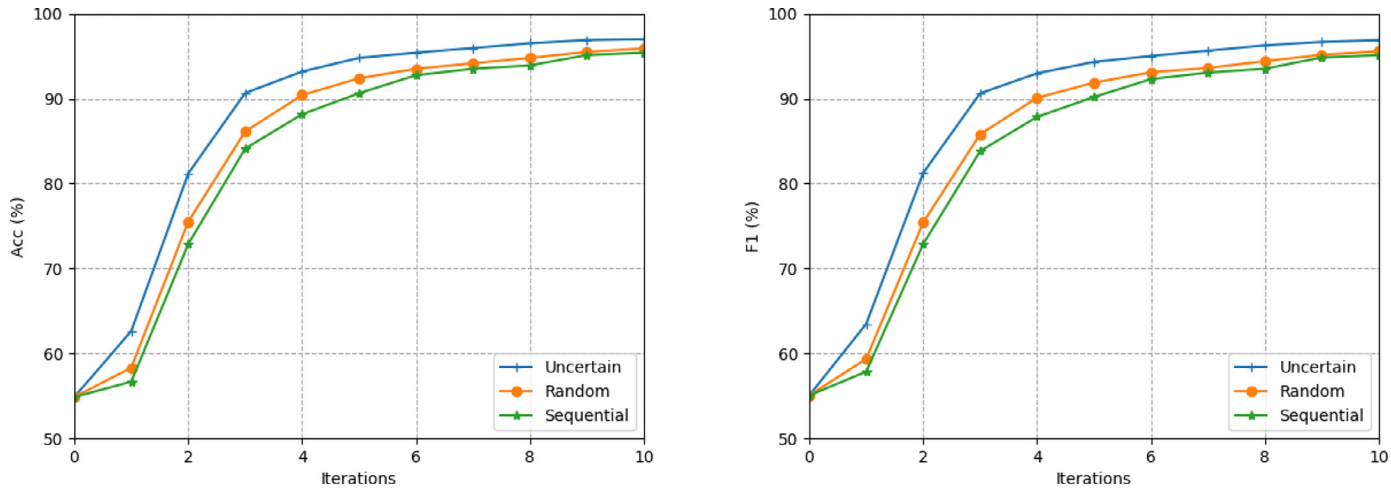


Fig. 7. Model updates based on different sampling strategies.

Table 8

Confusion matrix and performance across 5-fold cross validation based on intra-patient scheme using PTB and PTB-XL.

		Predicted						Performance				
		HC	ALMI	AMI	ASMI	ILMI	IMI	Acc (%)	Se (%)	Sp (%)	Pp (%)	F1 (%)
True	HC	31,047	22	489	310	44	556	97.05	95.62	97.60	93.88	94.75
	ALMI	267	7782	318	203	425	82	98.27	85.73	99.32	91.46	88.50
	AMI	138	117	6970	580	24	93	97.73	87.98	98.44	80.48	84.06
	ASMI	374	416	704	27,429	893	206	96.10	91.36	97.75	93.36	92.35
	ILMI	572	83	22	264	10,494	660	96.27	86.76	97.37	79.24	82.83
	IMI	672	89	158	594	1364	22,139	96.16	88.50	98.26	93.27	90.82
		Overall						90.79	89.33	98.12	88.61	88.89

quires fewer samples to be labeled for the same effect, reducing manual labeling labor.

4.4. Experimental results on PTB and PTB-XL

To further test the proposed method, the PTB and PTB-XL databases are combined to evaluate the proposed method under the intra-patient and the patient-specific schemes.

4.4.1. Intra-patient scheme

For the intra-patient scheme experiment, PTB and PTB-XL were mixed to perform 5-fold cross validation. The detailed classification results are shown in Table 8. The Acc, Se, Sp, Sp and F1 of the overall model is 90.79%, 89.33%, 98.12%, 88.61% and 88.89% respectively. The overall accuracy rate is 9% less than the result in Table 5. From the distribution of the confusion matrix, it can be seen that some MI samples are misdiagnosed as N, except that similar diseases are misclassified. It may be caused by the following reasons: i) Many MI samples in the PTB-XL database are subacute or old MI, while most of the data in PTB are acute MI. There may be differences in ECG performance of MI in different periods. ii) Most records in PTB-XL have multiple labels, that is, a sample may contain multiple diseases, which also leads to an increase in classification difficulty. iii) The ECG record length in the PTB-XL is only 10s, which is likely to cause different patients in the training set and test set, so the model is challenged by individual differences. Nevertheless, the Se of HC still reached 95.62%. In general, although the differences between databases have increased the difficulty of classification, the model still achieves acceptable results.

4.4.2. Patient-specific scheme

The PTB-XL database is not suitable as a test set, because the samples of each patient are so small that it cannot provide enough

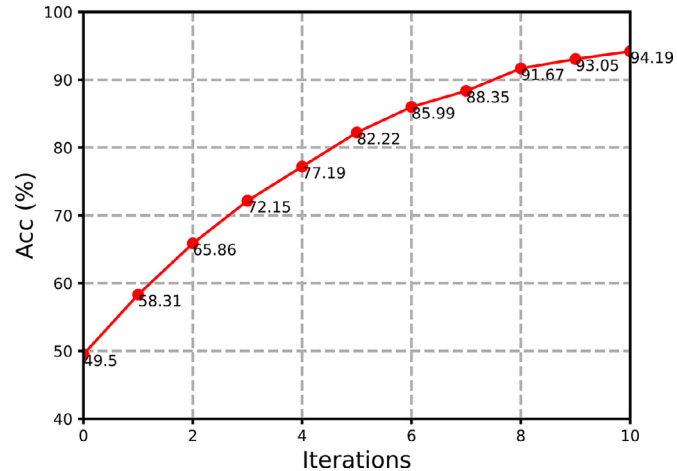


Fig. 8. Model update based on patient-specific scheme using PTB and PTB-XL.

unlabeled samples to implement AL strategies. Therefore, for the patient-specific scheme, PTB-XL is used as the initial training set, and the same patients from PTB in Section 4.3.2 are selected as the test set. Fig. 8 and Table 9 show the model optimization process and results based on AL under the patient-specific scheme. It can be seen that although the accuracy of the initial model is only 49.50% due to individual differences between patients and differences between the databases, it finally reaches 94.19% after 10 iterations. It reflects that the proposed optimization strategy can significantly improve the generalization ability of the model. Furthermore, this proves that the proposed method has the potential to be applied in real-world clinical medical diagnosis.

Table 9
Confusion matrix and performance based on patient-specific scheme using PTB and PTB-XL.

		Predicted						Performance				
		HC	ALMI	AMI	ASMI	ILMI	IMI	Acc (%)	Se (%)	Sp (%)	Pp (%)	F1 (%)
True	HC	844	0	0	0	0	19	98.30	97.80	98.36	87.92	92.59
	ALMI	11	913	128	60	0	2	97.28	81.96	99.78	98.38	89.42
AMI	16	15	1041	17	1	25	96.99	93.36	97.58	86.32	89.70	
ASMI	89	0	36	1448	0	4	97.38	91.82	98.76	94.83	93.30	
ILMI	0	0	0	0	1381	13	99.53	99.07	99.63	98.29	98.68	
IMI	0	0	1	2	23	1858	98.89	98.62	98.96	96.72	97.66	
		Overall						94.19	93.77	98.85	93.74	93.56

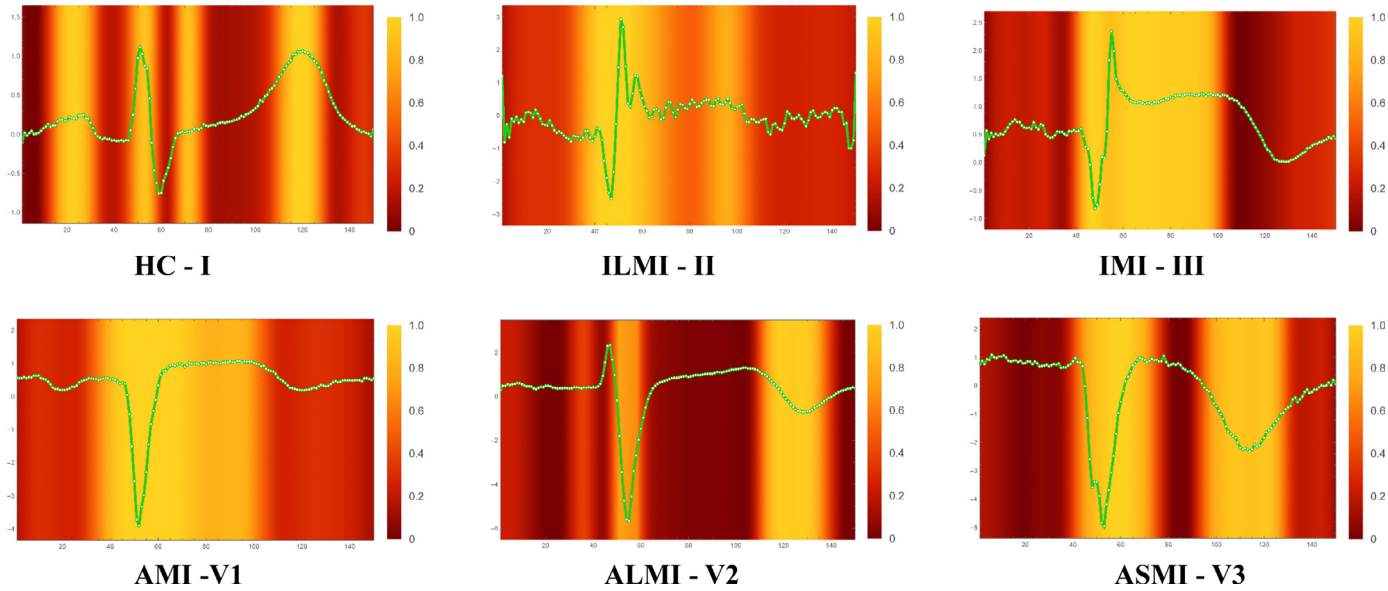


Fig. 9. Examples of heatmaps in MFB module.

5. Discussion

5.1. Visualization of learned features

Visualization is an important method to increase the interpretability of neural networks. In this subsection, we prove the effectiveness of the proposed model using visualization technology based on the intra-patient model.

The Grad-CAM [35] is widely used in the visual interpretation of neural network models. It can indicate which part of the original image the model is based on to lead the final classification result through the heat map. Based on this method, we verify which waveforms in the original signal have a greater impact on the final result. Fig. 9 shows the original signals of some leads and corresponding heat maps. The weight of the heat map is calculated based on the extracted features by the MFB module. The brighter the color in the figure, the higher the weight. From the HC sample in the figure, attention is mainly concentrated on P, QRS and T waves. For MI, it can be observed that the pathological QRS waves and ST-T changes are strongly activated, which shows that the features provide an important reference for the final decision of the model. Therefore, the MFB module can capture the key features inside the heartbeat. Furthermore, Fig. 10 shows the signal in lead II of different categories and the output of the third pooling layer in the corresponding branch. It can be seen that there are different degrees of pathological Q waves, ST-segment elevation, and T-wave inversion in the original MI signal. For the same input signal, the corresponding 16 feature maps are unique and abstract. This is because that randomly initialized weights cause different convolution kernels to have different parameters. During the training process, each convolution kernel has a different tendency and their parameters are getting more and more different. Therefore, different convolution kernels produce different outputs for the same input, and the model learns abstract features after three convolution and pooling operations.

Additionally, the relationship between leads is an important feature for the model to distinguish different types of MI. Thus, we proposed the LAM to obtain the weight contribution of different leads for samples of different categories. Given typical examples of AMI and IMI, the lead weight distribution and raw signals are shown as Fig. 11. For AMI, the typical symptoms are usually expressed in leads V1-V4 according to lead position distribution and MI diagnosis rules. It can be seen from the weight distribution that the corresponding lead weight is higher. Moreover, Leads aVL, aVF, I, II and III also play an important role, which may be used to exclude other categories. As for IMI, the symptoms above are usually shown in lead II, III, and aVF. According to the corresponding weight distribution and the original signal, the model can automatically extract the contribution of different leads to the recognition of IMI. The weight of the lead is multiplied by the corresponding feature branch output, which can strengthen the feature of the key leads and weaken the other leads to improve the diagnostic effect. Thus, LAM is an effective model optimization method for diagnosing multi-class MI.

Finally, the features extracted from different branches are aggregated to the fully connected layer after attention weighting. To further prove the contribution of the features, we extracted the output of the sample in the final FC layer, and t-SNE [36] was used

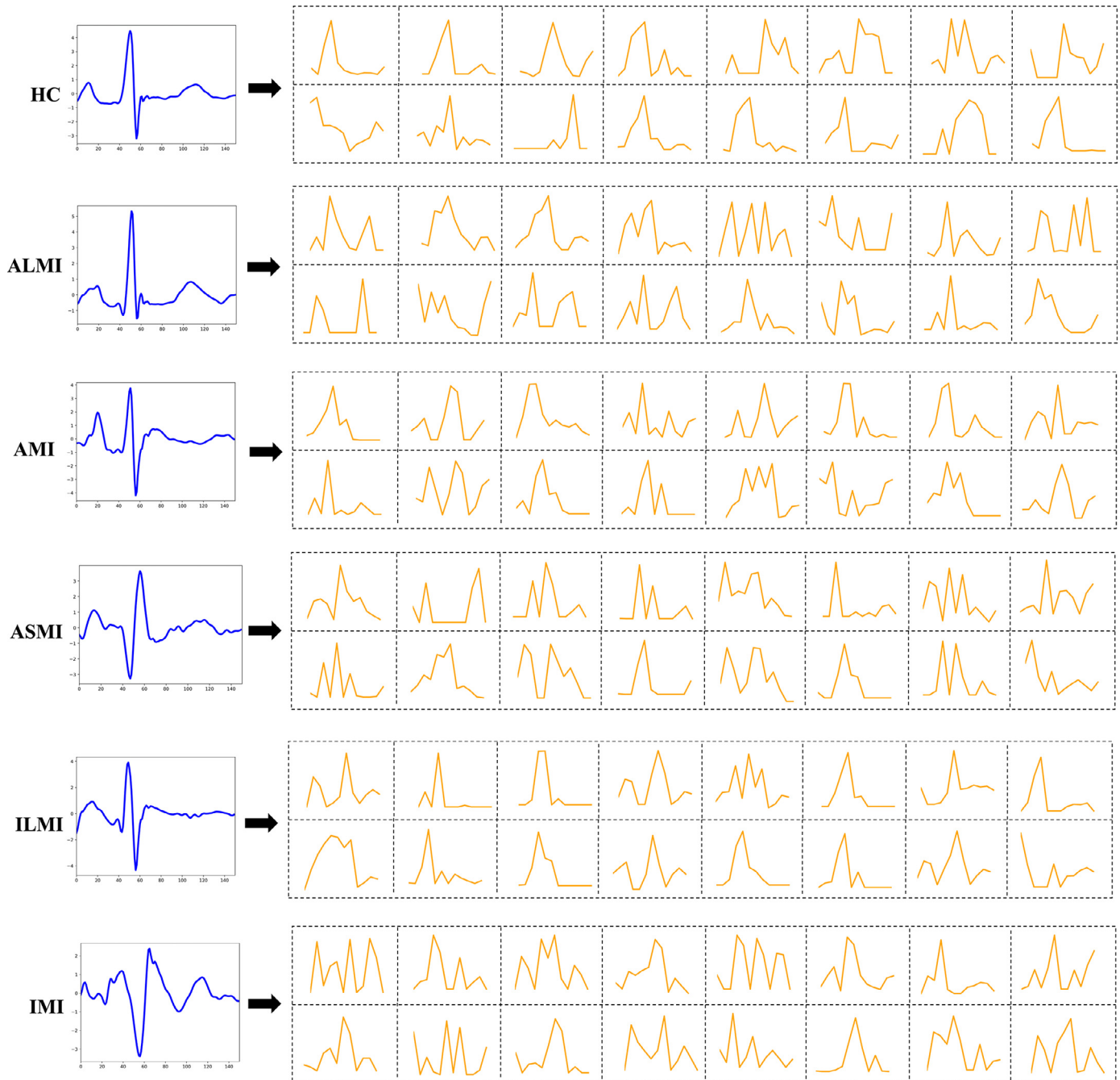


Fig. 10. The signal in lead II of different categories and the output of the third pooling layer in the corresponding branch.

to visualize these features. As shown in Fig. 12, almost all samples of the same category are projected to the same area. Only a few samples are misclassified and the result is consistent with the distribution of the confusion matrix in Table 5. Overall, the proposed model can extract valuable features.

5.2. Lightweight evaluation

Whether the model can run on resource-constrained edge devices is a major factor to be considered in mobile healthcare. Model parameters and computational complexity determine the operating platform and diagnosis time. In this paper, we mainly performed the following operations to implement the proposed lightweight model. i):The original signal is downsampled to reduce the depth of the model and the size of the convolution ker-

nel. ii):Depth separable convolution is used instead of traditional convolution. iii):The input dimension of FC in LAM module is compressed. iv):The dimensionality of feature maps is reduced through pooling layers. The total amount of the proposed model parameters is 5304, which is mainly determined by convolution layers and FC layers. The computational complexity affects the running speed of the model, which can be expressed as floating-point operations (FLOPs). According to the calculation method in [37], we can compute the FLOPs for 1-D convolution as follows:

$$F_C = 2L(C_{in}K + 1)C_{out} \quad (12)$$

$$F_{DWC} = 2LC_{in}(K + 1) \quad (13)$$

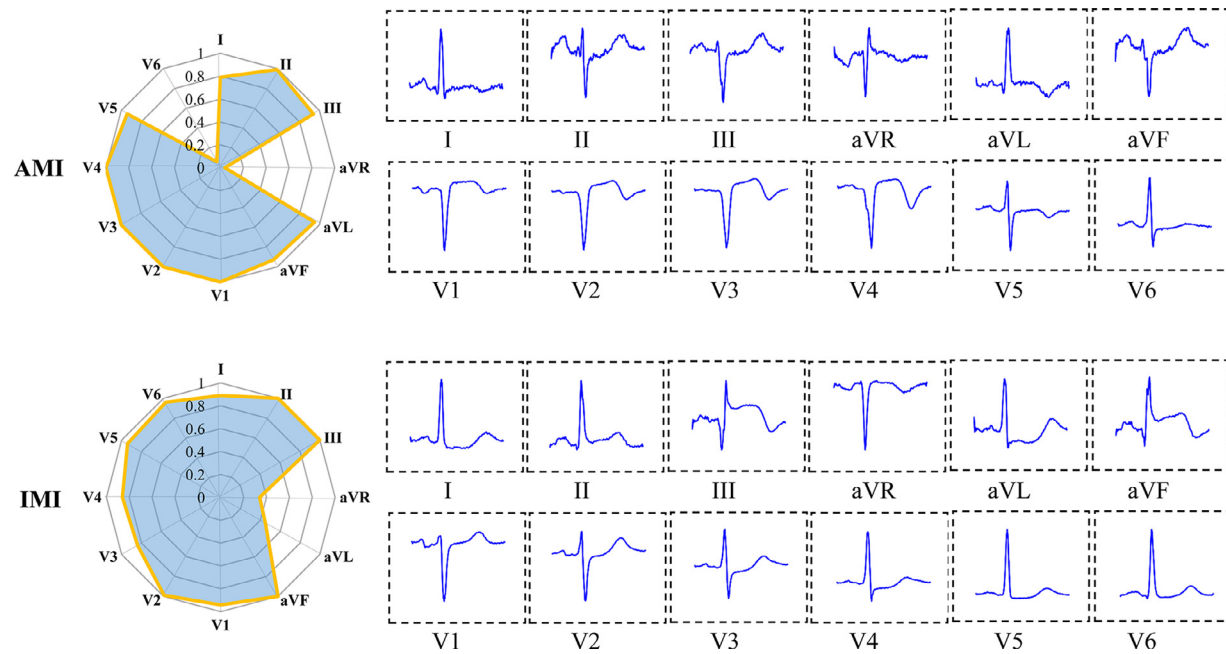


Fig. 11. Examples of Lead weights for typical AMI and IMI in LAM module.

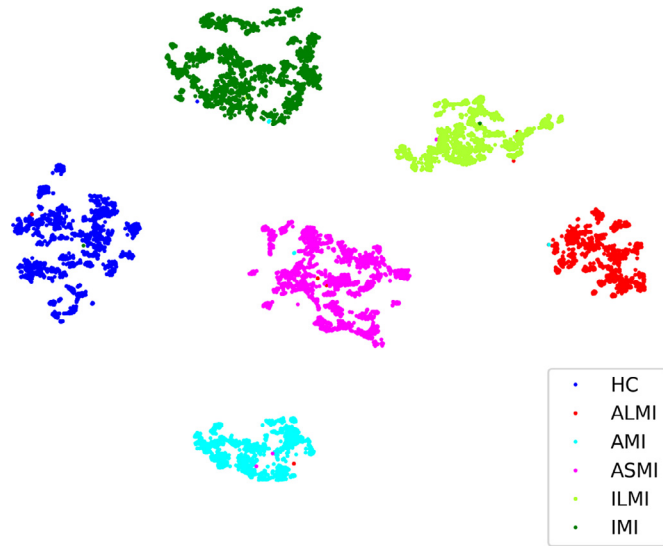


Fig. 12. The t-SNE visualization. (The features of the final FC layer are projected on a two-dimensional plane after dimensionality reduction).

$$F_{PWC} = 2L(C_{in} + 1)C_{out} \quad (14)$$

where F_C , F_{DWC} , F_{PWC} represent the FLOPs of different convolution types. L , C_{in} , K , C_{out} are the length of the input, the number of input channels, the length of the convolution kernel, and the number of output channels. For FC as follows:

$$F_{FC} = (2I - 1)O \quad (15)$$

where I and O are the input dimensionality and output dimensionality. According to the above formula, the FLOPs of the proposed model is about 0.47 MFLOPs. The specific calculation process of parameters and FLOPs is shown in Table 10. Compared with the neural network models in [38] that can run on resource-constrained edge devices, MFB-LANN has obvious advantages in parameters and FLOPs. For example, it takes 23ms for MobileNet to classify

Table 10
Parameter and FLOPs for MFB-LANN.

Layer	Parameters	FLOPs
MFB module	C	$12 \times 2 \times 150 \times (17+1) \times 4$
	DWC	$12 \times 2 \times 50 \times (9+1) \times 4$
	PWC	$12 \times 2 \times 50 \times (4+1) \times 8$
	DWC	$12 \times 5 \times 8$
	PWC	$12 \times 8 \times 16$
	C	12×16
	FC	$(2 \times 12-1) \times 12$
	FC	$(2 \times 12 \times 16-1) \times 6$
	Total	5304
		473,670

C: Traditional convolutional; DWC: Depthwise convolution; PWC: Pointwise convolution; FC: Fully connected.

an image with a size of 224x224 on a smart phone. Its parameters and FLOPs are 4.2M and 1.14GFLOPs, which are larger than our proposed model.

In addition, we deployed the proposed model on personal computer (PC) and Raspberry Pi (RPi). RPi with ARM processor is a system on chip (SOC) device compared to traditional PC, and it is the most widely used embedded framework in real-world applications. The same operating environment is deployed on the devices. The test procedure of the proposed method on RPi is shown in Fig. 13. First, the MFB-LANN is pre-trained on the AI server to form the initial model. At the same time, The ECG signal of the new patient are stored on the SD card of the RPi for model update and diagnosis respectively. Finally, the data and model are loaded by the ARM processor and RAM. 100 unlabeled samples and 100 labeled samples are used to test model update time and classification time. The detailed equipment configuration and experimental results are shown in Table 11. For model on PC, it takes 28.06s to complete a model update process, and the average classification time of each heartbeat is 38ms. On the contrary, the model on the RPi is relatively time-consuming due to the limited processor and memory, model update time and average classification time are 1168s and 102ms, respectively. Thus, the computational cost is significantly less than the duration of the heartbeat, which demonstrated that the algorithm could realize real-time diagnosis [39]. Moreover, the

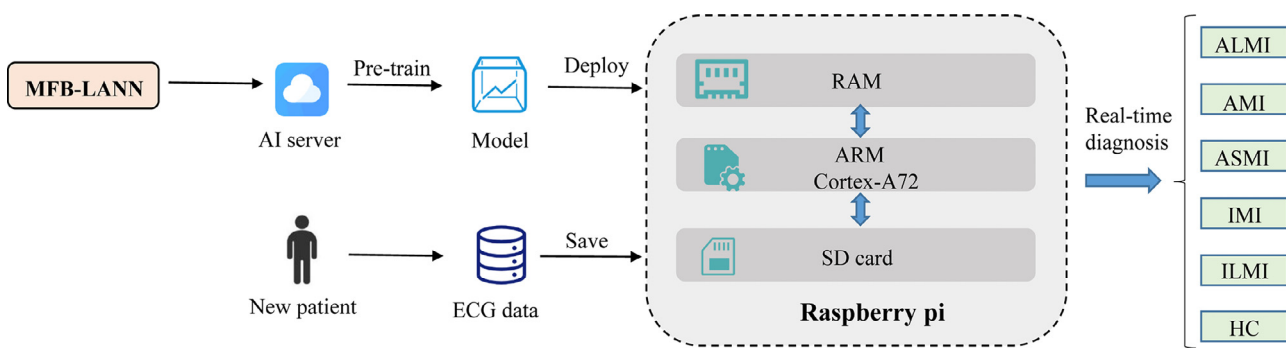


Fig. 13. Flow chart of the proposed system deployment on embedded devices.

Table 11

Time consumption of MFB-LANN on different devices.

Device	Configuration	Update time	Classification time
PC	Intel Core i5-7400@3.00 GHz CPU and 8 GB RAM	28.06s	38ms
Rpi	1.5GHz quad-core ARM Cortex-A72 CPU and 4GB RAM	1168s	102ms

PC: personal computer; RPi: Raspberry Pi.

Table 12

Comparison of the proposed method against existing methods for MI diagnosis.

Study	Method	No. of hand-crafted features	No. of classes	Intra-patient	Patient-specific	Parameters	MFLOPs
2016 [2]	MEES+SVM	72	6	Acc = 99.58%	NA	NA	NA
2016 [12]	DWT+KNN	25	11	Acc = 98.74%, Se = 99.55%, Sp = 99.16%	NA	NA	NA
2018 [19]	MFB-CNN	0	6	Acc = 99.81%	Acc = 94.82%	6372	1.27
2019 [15]	ML-ResNet	0	6	Acc = 99.72%, Se = 99.63%, Sp = 99.72%, F1 = 99.67%	NA	18096	4.93
2021 [40]	DenseNet	0	12	Acc = 99.87%, Se = 99.84%, Sp = 99.98%	NA	NA	NA
2021 [5]	DWT+PFA+BDT	36	12	Acc = 99.40%, Se = 99.86%, Sp = 99.89%	NA	NA	NA
Proposed	MFB-LANN	0	6	Acc = 99.63%, Se = 99.61%, Sp = 99.93%, Pp = 99.56%, F1 = 99.59%	Acc = 96.99%, Se = 96.86%, Sp = 99.40%, Pp = 96.87%, F1 = 96.87%	5304	0.47

MEES: Multiscale Energy and Eigenspace; SVM: Support Vector Machine; DWT: Discrete Wavelet Transform; KNN: K-Nearest Neighbor; MFB-CNN: Multiple-feature-branch Convolutional Neural Network; ML-ResNet: Multi-lead Residual Neural Network; DenseNet: Densely connected network; PFA: Parallel Factor Analysis; BDT: Bagged decision tree; MFB-LANN: Multi-feature-branch Lead Attention Neural Network.

update process needs to train the model through backpropagation, which consumes more hardware resources than the classification process. The proposed model can complete the update process on the RPi, which further proves its lightweight advantage.

5.3. Comparisons with state-of-the-art results

To demonstrate the advantages of our proposed model, Table 12 summarizes the research results of the proposed method and recent methods for MI multi-category diagnosis based on the PTB database. The methods proposed in [2,5,12] are based on traditional machine learning, which requires manual extraction features. For example, Sharma et al. [2] proposed a novel technique on a multiscale energy and eigenspace (MEES) approach to extract 72 features, and finally achieved 99.58% accuracy by SVM. Although methods based on traditional machine learning have achieved good results under the intra-patient scheme, the classification process is more complicated. By contrast, the classification process based on deep learning methods is automatic. Moreover, for a comprehensive comparison, we calculated the parameters and FLOPs of other neural network models except [40] which did not provide detailed convolution configuration. Xiong et al. [40] designed a novel multi-lead MI localization model based on the densely con-

nected network (DenseNet), which achieved 99.87% accuracy under the intra-patient scheme. Similarly, Han et al. [15] proposed a multi-lead residual neural network (ML-ResNet) achieved an accuracy of 99.72%, but the patient-specific experiment has not been performed. Furthermore, it can be seen from the table that the model in [19] based on the patient-specific framework considered individual differences and achieved acceptable results by the fine-tuning process. However, as mentioned before, the sequential sampling method cannot guarantee that the selected data is the most representative, which is likely to cause waste labeling labor and limit the maximum capacity of the model in practical applications. In addition, these methods do not consider the computational complexity and parameters of the algorithms, and the authors did not test the model on resource-constrained edge device.

Compared with the above method, it can be observed that the MFB-LANN has the following advantages. Firstly, MFB-LANN is an end-to-end automatic MI diagnosis system based on DL. The architecture satisfies the ECG lead characteristics. It has 12 feature branches with the same structure that can extract the features of the 12 leads. In particular, the LAM can automatically learn the contribution distribution of different leads to different samples. According to the experiment based on the intra-patient scheme in this paper, the model can extract useful waveform features and

lead relationship distribution, and finally achieved an accuracy of 99.63% based on 5-fold cross validation. Although the result is about 0.1% lower than the models in [19] and [15], the proposed model has fewer parameters and FLOPs. For example, the parameters and FLOPs of MFB-LANN are only one-third and one-tenth of ML-ResNet [15]. Secondly, for individual differences between patients, MFB-LANN is trained and updated based on patient-specific scheme and AL strategies, and it can gradually adapt to the characteristics of new patient data in the iterative optimization process. The uncertainty sampling strategy ensures that the data selected in each iteration is valuable to improve the model effect with fewer samples and faster speed. The final model achieved satisfactory results under patient-specific scheme, which proves the effectiveness of the proposed optimization strategy. Thirdly, MFB-LANN is a lightweight model. Its parameters and computational complexity are 5304 and 0.47MF-LOPs, which reduces the limitation on the operating platform. Especially we successfully implemented the model update process and real-time diagnosis process on RPi. In general, MFB-LANN has impressive advantages and achieves significant results, which indicates that it is an effective MI diagnosis system.

6. Conclusion

In this paper, a lightweight neural network model called MFB-LANN is proposed to diagnose MI using 12 leads ECG signals. Its structure conforms to the characteristics of ECG leads and can capture useful features. Specifically, 12 independent convolution branches respectively correspond to 12 leads to extract the internal features of the heartbeat, and a new LAM is designed to obtain the weight distribution of different branches. All branch features are fused for final diagnosis, and the whole process is automatic without manual feature extraction. The model achieves the accuracy of 99.63% under the intra-patient scheme on PTB database, which proves the powerful fitting ability. In order to overcome individual differences, the model is trained based on patient-specific scheme. Also, the AL strategy is added to update the model iteratively, which can improve the model effect with fewer samples. The final model reached an accuracy of 96.99% on the new patients and achieved state-of-the-art performance on PTB database, and it achieves an accuracy of 94.19% using PTB and PTB-XL databases. Moreover, MFB-LANN is a lightweight architecture, and experiments have proved that it can complete the update process and real-time diagnosis on RPi. In general, MFB-LANN is very potential as an MI diagnosis system for mobile medical applications. Currently, the proposed system has not been used for clinical verification.

In the future, we will cooperate with hospitals and further expand the diagnostic functions of the model. First, labeled ECG data containing more types of MI in the hospital database or in the public database are used to train the initial MFB-LANN model. Then, for new patients, the AL strategy is used to update the model. Finally, the final model is used to diagnose MI for these new patients, and cardiologists will help verify the system results. At the same time, we will combine with wearable ECG acquisition devices to realize an ECG real-time diagnostic system in the real-world.

Declaration of Competing Interest

The authors declare that they have no known competing financial interests or personal relationships that could have appeared to influence the work reported in this paper.

Acknowledgment

As follows Acknowledgment This work was supported in part by the National Natural Science Foundation of China (No. 62073248), in part by the Translational Medicine and Interdisciplinary Research Joint Fund of Zhongnan Hospital of Wuhan University (No. ZNJC201926) under, in part by the Science and Technology Major Project of Hubei Province, China (Next Generation AI Technologies, No. 2019AEA170). Zhiyong Yuan and Jianhui Zhao are corresponding authours. All authors read and contributed to the paper.

References

- [1] J.H. Joloudari, S. Mojrian, I. Nodehi, A. Mashmool, Z.K. Zadegan, S.K. Shirkharkolaie, T. Tamadon, S. Khosravi, M. Akbari, E. Hassannataj, et al., A survey of applications of artificial intelligence for myocardial infarction disease diagnosis, arXiv preprint arXiv:2107.06179 (2021).
- [2] L.N. Sharma, R.K. Tripathy, S. Dandapat, Multiscale energy and eigenspace approach to detection and localization of myocardial infarction, IEEE Trans. Biomed. Eng. 62 (7) (2015) 1827–1837.
- [3] J.J. Bax, H. Baumgartner, C. Ceconi, V. Dean, R. Fagard, C. Funck-Brentano, D. Hasdai, A. Hoes, P. Kirchhof, J. Knuuti, et al., Third universal definition of myocardial infarction, J. Am. Coll. Cardiol. 60 (16) (2012) 1581–1598.
- [4] S. Kaplan Berkaya, A.K. Uysal, E. Sora Gunal, S. Ergin, S. Gunal, M.B. Gulmezoglu, A survey on ecg analysis, Biomed Signal Process Control 43 (2018) 216–235.
- [5] J. Zhang, M. Liu, P. Xiong, H. Du, H. Zhang, F. Lin, Z. Hou, X. Liu, A multi-dimensional association information analysis approach to automated detection and localization of myocardial infarction, Eng Appl Artif Intell 97 (2021) 104092.
- [6] C. Sridhar, O.S. Liu, V. Jahmunah, J.E. Koh, E.J. Ciaccio, T.R. San, N. Arunkumar, S. Kadry, U.R. Acharya, Accurate detection of myocardial infarction using non linear features with ecg signals, J Ambient Intell Humaniz Comput 12 (3) (2021) 3227–3244.
- [7] B. Fatimah, P. Singh, A. Singhal, D. Pramanick, S. Pranav, R.B. Pachori, Efficient detection of myocardial infarction from single lead ecg signal, Biomed Signal Process Control 68 (2021) 102678.
- [8] A.K. Dohare, V. Kumar, R. Kumar, Detection of myocardial infarction in 12 lead ecg using support vector machine, Appl Soft Comput 64 (2018) 138–147.
- [9] C. Han, L. Shi, Automated interpretable detection of myocardial infarction fusing energy entropy and morphological features, Comput Methods Programs Biomed 175 (2019) 9–23.
- [10] M. Kumar, R.B. Pachori, U.R. Acharya, Automated diagnosis of myocardial infarction ecg signals using sample entropy in flexible analytic wavelet transform framework, Entropy 19 (9) (2017) 488.
- [11] S. Padhy, S. Dandapat, Third-order tensor based analysis of multilead ecg for classification of myocardial infarction, Biomed Signal Process Control 31 (2017) 71–78.
- [12] U.R. Acharya, H. Fujita, V.K. Sudarshan, S.L. Oh, M. Adam, J.E.W. Koh, J.H. Tan, D.N. Ghista, R.J. Martis, C.K.a. Chua, Automated detection and localization of myocardial infarction using electrocardiogram: a comparative study of different leads, Knowl Based Syst 99 (may1) (2016) 146–156.
- [13] A. Chen, F. Wang, W. Liu, S. Chang, H. Wang, J. He, Q. Huang, Multi-information fusion neural networks for arrhythmia automatic detection, Comput Methods Programs Biomed (2020) 105479.
- [14] U.R. Acharya, H. Fujita, S.L. Oh, Y. Hagiwara, J.H. Tan, M. Adam, Application of deep convolutional neural network for automated detection of myocardial infarction using ecg signals, Inf Sci (Ny) 415 (2017) 190–198.
- [15] C. Han, L. Shi, Mi-resnet: a novel network to detect and locate myocardial infarction using 12 leads ecg, Comput Methods Programs Biomed 185 (2019) 105138.
- [16] U.B. Baloglu, M. Talo, O. Yildirim, R. San Tan, U.R. Acharya, Classification of myocardial infarction with multi-lead ecg signals and deep cnn, Pattern Recognit Lett 122 (2019) 23–30.
- [17] W. Liu, F. Wang, Q. Huang, S. Chang, H. Wang, J. He, Mfb-cbrnn: a hybrid network for mi detection using 12-lead ecgs, IEEE J Biomed Health Inform 24 (2) (2019) 503–514.
- [18] T. Reasat, C. Shahnaz, Detection of inferior myocardial infarction using shallow convolutional neural networks, in: 2017 IEEE Region 10 Humanitarian Technology Conference (R10-HTC), IEEE, 2017, pp. 718–721.
- [19] W. Liu, Q. Huang, S. Chang, H. Wang, J. He, Multiple-feature-branch convolutional neural network for myocardial infarction diagnosis using electrocardiogram, Biomed Signal Process Control 45 (AUG.) (2018) 22–32.
- [20] A.L. Goldberger, L.A. Amaral, L. Glass, J.M. Hausdorff, P.C. Ivanov, R.G. Mark, J.E. Mietus, G.B. Moody, C.-K. Peng, H.E. Stanley, Physiobank, physiotoolkit, and physionet: components of a new research resource for complex physiologic signals, Circulation 101 (23) (2000) e215–e220.
- [21] P. Wagner, N. Strodthoff, R.-D. Bousseljot, D. Kreiseler, F.I. Lunze, W. Samek, T. Schaeffer, Ptb-xl, a large publicly available electrocardiography dataset, Sci Data 7 (1) (2020) 1–15.
- [22] J. Pan, W.J. Tompkins, A real-time qrs detection algorithm, IEEE Trans. Biomed. Eng. (3) (1985) 230–236.

- [23] A.G. Howard, M. Zhu, B. Chen, D. Kalenichenko, W. Wang, T. Weyand, M. Andreetto, H. Adam, Mobilenets: efficient convolutional neural networks for mobile vision applications, arXiv preprint arXiv:1704.04861 (2017).
- [24] G. Tang, M. Müller, A. Rios, R. Sennrich, Why self-attention? a targeted evaluation of neural machine translation architectures, arXiv preprint arXiv:1808.08946 (2018).
- [25] J. Hu, L. Shen, G. Sun, Squeeze-and-excitation networks, in: Proceedings of the IEEE conference on computer vision and pattern recognition, 2018, pp. 7132–7141.
- [26] X. Glorot, A. Bordes, Y. Bengio, Deep sparse rectifier neural networks, Journal of Machine Learning Research 15 (2011) 315–323.
- [27] G.E. Hinton, N. Srivastava, A. Krizhevsky, I. Sutskever, R.R. Salakhutdinov, Improving neural networks by preventing co-adaptation of feature detectors, Computer Science 3 (4) (2012) pgs.212–223.
- [28] S. Kiranyaz, T. Ince, M. Gabbouj, Real-time patient-specific ecg classification by 1-d convolutional neural networks, IEEE Trans. Biomed. Eng. 63 (3) (2016) 664–675.
- [29] X. Dong, C. Wang, W. Si, Ecg beat classification via deterministic learning, Neurocomputing 240 (May31) (2017) 1–12.
- [30] M.M. Al Rahhal, Y. Bazi, H. AlHichri, N. Alajlan, F. Melgani, R.R. Yager, Deep learning approach for active classification of electrocardiogram signals, Inf Sci (Ny) 345 (2016) 340–354.
- [31] G. Wang, C. Zhang, Y. Liu, H. Yang, D. Fu, H. Wang, P. Zhang, A global and updatable ecg beat classification system based on recurrent neural networks and active learning, Inf Sci (Ny) 501 (2019) 523–542.
- [32] W.-N. Hsu, H.-T. Lin, Active learning by learning, Twenty-Ninth AAAI conference on artificial intelligence, Citeseer, 2015.
- [33] A.J. Joshi, F. Porikli, N. Papanikolopoulos, Multi-class active learning for image classification, in: 2009 IEEE Conference on Computer Vision and Pattern Recognition, IEEE, 2009, pp. 2372–2379.
- [34] D.P. Kingma, J. Ba, Adam: a method for stochastic optimization, arXiv preprint arXiv:1412.6980 (2014).
- [35] R.R. Selvaraju, M. Cogswell, A. Das, R. Vedantam, D. Parikh, D. Batra, Grad-cam: Visual explanations from deep networks via gradient-based localization, in: Proceedings of the IEEE international conference on computer vision, 2017, pp. 618–626.
- [36] S. Arora, W. Hu, P.K. Kothari, An analysis of the t-sne algorithm for data visualization, in: Conference On Learning Theory, PMLR, 2018, pp. 1455–1462.
- [37] P. Molchanov, S. Tyree, T. Karras, T. Aila, J. Kautz, Pruning convolutional neural networks for resource efficient inference, arXiv preprint arXiv:1611.06440 (2016).
- [38] A. Ignatov, R. Timofte, W. Chou, K. Wang, M. Wu, T. Hartley, L. Van Gool, Ai benchmark: Running deep neural networks on android smartphones, in: Proceedings of the European Conference on Computer Vision (ECCV), 2018, 0–0.
- [39] W. Liu, M. Zhang, Y. Zhang, Y. Liao, Q. Huang, S. Chang, H. Wang, J. He, Real-time multilead convolutional neural network for myocardial infarction detection, IEEE J Biomed Health Inform 22 (5) (2017) 1434–1444.
- [40] P. Xiong, Y. Xue, J. Zhang, M. Liu, H. Du, H. Zhang, Z. Hou, H. Wang, X. Liu, Localization of myocardial infarction with multi-lead ecg based on densenet, Comput Methods Programs Biomed 203 (2021) 106024.